PERGAMON

International Journal of Heat and Mass Transfer 43 (2000) 493–504

International Journal of HEAT and MASS TRANSFER

www.elsevier.com/locate/ijhmt

Conductive mass transport from a semi-infinite lattice of particles

C. Pozrikidis*

University of California, San Diego, La Jolla, CA 92093-0411, USA

Received 19 November 1998; received in revised form 30 April 1999

Abstract

A method is presented for computing the instantaneous rate of conductive mass transport from a semi-infinite lattice of particles with arbitrary shape, in the limit as the particle size becomes small compared to the particle separation. A fixed rate of transport is imposed above the lattice, and the concentration is assumed to be constant and uniform over the particles' surface. Transport due to forced or natural convection is neglected, and the particle dissolution or evaporation is assumed to be limited by diffusion. In the mathematical formulation, the concentration field induced by each particle layer is expressed in terms of the doubly-periodic Green's function of Laplace's equation in three dimensions, which is evaluated using either a Fourier series or an alternative representation involving rapidly converging Ewald sums. The rate of transport from each layer is found using the method of matched asymptotic expansions resulting in a system of linear algebraic equations. Numerical results are presented for lattices with different configurations at various particle volume fractions, showing exponential decay of the rate of transport with distance from the top layer, in agreement with theoretical predictions. Having obtained general expressions for the rate of transport, a system of differential equations governing the evolution of the radii of dissolving spherical particles is derived. Numerical solutions illustrate the distribution of the particle radii after a periodic state has been established.

1. Introduction

Evaporation of a particulate solid is a fundamental process of mass transfer with a variety of natural and industrial applications. Under typical conditions, the evaporating species diffuses through a sparse or consolidated matrix of particles and enters the ambience under the influence of an externally imposed concentration gradient. A similar process occurs during the drying of a porous medium or a concentrated suspension such as a paste or a photographic emulsion. During the late stages of drying, the liquid phase forms disconnected globules that are supported by an underlying fiber or particle network, and diffusion occurs through the interstitial spaces and into the dry environment.

Conductive transport across a particulate medium has been studied on many occasions with the main goal of estimating the effective medium conductivity or diffusivity as a function of the particulate phase microstructure and volume fraction (e.g. [1,2]). In the mathematical modeling, the medium is often assumed to be spatially periodic and thus represented by a triply-periodic particle array embedded in a matrix. In the limit of small volume fractions, the analysis is conducted using the method of matched asymptotic expansions. Models of evaporation or drying of a particulate medium of finite extent are typically based on the con-

* Tel.: +1-858-534-6530; fax: +1-858-534-7078.
E-mail address: cpozrikidis@ucsd.edu (C. Pozrikidis)

0017-9310/00/$ - see front matter
PII: S0017-9310(99)00163-5

Nomenclature

a_l	typical size or radius of spherical particles in the lth layer
$\mathbf{a}_i$	base vectors of the Bravais lattice, $i = 1, 2, 3$
A	surface area of a planar lattice cell
$\mathbf{b}_i$	base vectors of the reciprocal (wave number) lattice
B	bottom of control volume
c	concentration
c_0	concentration at the particle surface
c_D	displacement constant of the concentration profile
$c_{-\infty}$	concentration far below a lattice comprised of a finite number of layers
$\mathbf{e}_i$	unit vectors along three Cartesian axes, $i = 1, 2, 3$
d_k^{∞}	lattice configuration constant associated with the Green's function
D	mass diffusivity
G^{3D-2P}	Green's function of Laplace's equation
h_l	mass transfer coefficient of particles in the lth layer
L	characteristic lattice size
m	molecular weight
$\mathbf{M}$	influence matrix
$\mathbf{n}$	unit normal vector pointing outward from the particles
NLR	number of particle layers
Nu_l	Nusselt number for particles in the lth layer
$Nu_l^{Lattice}$	lattice Nusselt number for particles in the lth layer
p	pressure
P	particle surfaces
q^{∞}	mass flux far above the top layer
Q	rate of mass transport across a planar cell
Q_l	rate of mass transport from the particles in the lth layer
$\mathbf{s}$	projection of the position vector onto the plane of a lattice
S	surface area
T	top of a control volume
$\mathbf{x}$	position vector
$\mathbf{x}_0$	position vector
$\mathbf{X}_i$	location of the ith vertex of the Bravais lattice
$\mathbf{u}$	velocity vector

Greek symbols

δ	delta function in three dimensions
μ	fluid viscosity
ρ_l	density of particles in the lth layer
σ	rate of decay of the rate of transport down the lattice
ϕ	particle volume fraction in the matrix

Subscripts and superscripts

l, k	labels of particle layers numbered from the top
m, n	lattice node indices
3D–2P	three-dimensional and doubly-periodic
i	ranges over 1, 2, 3 or x, y, z
∞	indicates the far-field value

tinuum approximation that neglects the discrete nature of the medium across which transport takes place (e.g. [3]). The rate of change of thickness or position of the interface of the evaporating species is then computed by performing a one-dimensional material balance assuming a constant or position-dependent effective diffusivity. These models are adequate for rough engineering estimates, but fail to provide us with insights into the fundamental physical processes occurring on the level of the microstructure.

In the present paper, we study transport through a semi-infinite particulate medium with a well-defined interface, where the transport is due to a scalar gradient maintained far above the interface. The particulate phase consists of a fixed, but possibly evaporating, semi-infinite matrix of liquid or solid particles whose size is small compared to the inter-particle separation. Transport due to natural or forced convection is neglected, and the particle dissolution or evaporation is assumed to be limited by diffusion. Using the method of matched asymptotic expansions, whose implementation requires the availability of the doubly-periodic Green's function of Laplace's equation in three dimensions, we derive expressions for the rate of transport from the particles, and then develop evolution equations for the particle size.

An analogy exists between the problem presently considered, and the problem of shear flow over a semi-infinite porous medium modeled as a semi-infinite matrix of rigid particles. The drag force exerted on the particles in the fluid flow problem is the counterpart of the rate of mass transport in the present problem. Larson and Higdon [4,5] presented numerical results for axial and transverse flow through a semi-infinite lattice of cylinders, obtained by a boundary-integral method, and discussed the relevance of Brinkman's

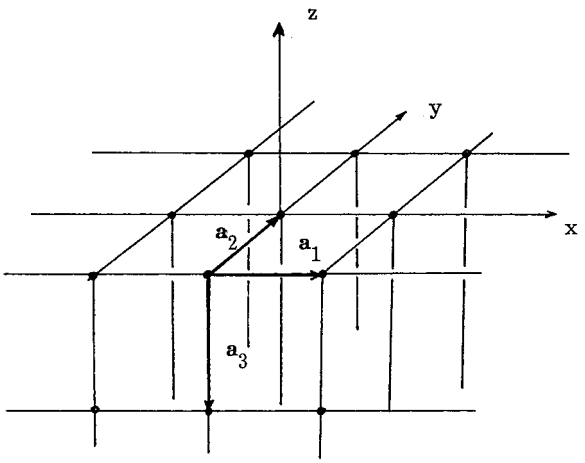

Fig. 1. A model medium consisting of a semi-infinite lattice of particles arranged in parallel layers. Mass transport occurs through the layers and into the overlying ambience. The concentration at the particle surface is assumed to be constant.

equation near the interface. In the case of axial flow, the non-zero velocity component satisfies the two-dimensional Laplace equation with homogeneous boundary conditions imposed around the cylinder contours. Thus, the numerical results of Larson and Higdon [4] may be reinterpreted in the present context of conductive transport from fibrous particles with cylindrical shapes. Most relevant to the present problem is the work of Sangani and Behl [2] who considered thermal conduction from a semi-infinite matrix of spherical particles, as well as diffusion accompanied by chemical reaction occurring either in the interior or on the surface of the particles. The present problem formulation and results are complementary to the ones presented by the previous authors.

2. Mathematical formulation

Consider mass transport across the surfaces of an infinite number of particles located at the nodes of a semi-infinite lattice, as illustrated in Fig. 1. The nodes of the lattice are located the points $\mathbf{x}_n = \mathbf{x}_0 + \mathbf{X}_n$, where $\mathbf{x}_0$ is the position of any one node. The vectors $\mathbf{X}_n$ define the vertices of a three-dimensional semi-infinite Bravais lattice described by

$$\mathbf{X}_n = i_1\mathbf{a}_1 + i_2\mathbf{a}_2 + i_3\mathbf{a}_3 \tag{1}$$

where $\mathbf{a}_1$, $\mathbf{a}_2$, $\mathbf{a}_3$ are three specified base vectors. The integers i_1 and i_2 take values from $-\infty$ to ∞, whereas the integer i_3 takes values over a semi-infinite set of integers describing the semi-infinite lattice.

Without loss of generality, we use Cartesian axes with the xy or 12 plane parallel to the plane that contains $\mathbf{a}_1$ and $\mathbf{a}_2$, which is designated as the horizontal plane. The areas of the planar cells corresponding to different particle layers are not necessarily equal, but the structure of the layers must be such that the periodicity of the concentration field conforms with that of the top-layer. For simplicity, however, we shall assume that the three base vectors are constant and the areas of the planar cells are equal to A.

Particles that lie in a horizontal layer corresponding to a particular value of the index i_3 introduced in (1) are assumed to be identical in shape and size, but variations are allowed across different layers down the matrix. The concentration c of a species at the surface of each particle is assumed to be uniform and equal to c_0. For the applications we have in mind, c_0 may be identified with the vapor pressure of the solid or liquid material comprising the particles. In the intervening space, the species concentration satisfies Laplace's equation $\nabla^2 c = 0$. Mass is transported through successive layers toward the top layer and then into the semi-infinite ambience above the matrix. The concentration field far above the top layer takes the asymptotic form

$$c = -\frac{q^\infty}{D} z + c_{\mathrm{D}} + \mathrm{edt} \tag{2}$$

where q^∞ is the uniform flux far above the top layer, D is the species diffusivity, c_{D} is a displacement constant of the concentration profile corresponding to the designated origin of the z axis, and edt stands for 'exponentially decaying terms'. Far below the top layer, the rate of mass transport vanishes, and the concentration tends to the particle surface value c_0.

If the number of particle layers and thus the depth of the matrix were finite, the concentration far below the bottom layer would not tend to the particle surface value c_0, but would tend instead to another uniform value $c_{-\infty}$ that is higher than c_0. This asymptotic value cannot be specified in the statement of the problem but must be computed as part of the solution.

2.1. Integral representation

As a preliminary, we introduce the doubly-periodic Green's function of Laplace's equation in three dimensions, denoted as $G^{\mathrm{3D-2P}}(\mathbf{x}, \mathbf{x}_0)$, with dimensions of inverse length. By definition, this Green's function satisfies the singularly forced Laplace's equation

$$\nabla^2 G^{\mathrm{3D-2P}}(\mathbf{x}, \mathbf{x}_0) + \sum_{m,\, n=-\infty}^{\infty} \delta(\mathbf{x} - \mathbf{x}_{mn}) = 0 \tag{3}$$

where $\mathbf{x}_{mn}$ is the position of singularities in a planar lattice corresponding to a certain value of $i_3 = l$ in Eq.

(1), and δ is the three-dimensional delta function with dimensions of inverse cubed length. As the field point $\mathbf{x}$ moves far below the layer, $G^{3D-2P}(\mathbf{x}, \mathbf{x}_0)$ is required to vanish. As $\mathbf{x}$ moves far above the layer, the Green's function exhibits the asymptotic behavior

$$G^{3D-2P}(\mathbf{x}, \mathbf{x}_0) = -\frac{1}{A}(z - z_0) + \text{edt} \tag{4}$$

where A is the area of the planar cell. Because of these properties, the Green's function does not observe the usual invariance with respect to transposition of its argument, but satisfies instead the identity

$$G^{3D-2P}(\mathbf{x}, \mathbf{x}_0) = G^{3D-2P}(\mathbf{x}_0, \mathbf{x}) - \frac{1}{A}(z - z_0). \tag{5}$$

Two methods of computing $G^{3D-2P}(\mathbf{x}, \mathbf{x}_0)$ will be discussed in section 3.

Next, we select a control volume that contains one period of the semi-infinite lattice depicted in Fig. 1, with top and bottom surfaces located at large but finite distances above or below the top layer. For convenience, we assume that the top surface is horizontal. The concentration at a point $\mathbf{x}$ that is located within the control volume may be expressed in terms of a boundary integral representation as

$$c(\mathbf{x}) = -\int_{P,\,B,\,T} [\mathbf{n}\cdot\nabla c](\mathbf{x}_0)\; G^{3D-2P}(\mathbf{x}_0, \mathbf{x})\; dS(\mathbf{x}_0) + \int_{P,\,B,\,T} c(\mathbf{x}_0)\; \mathbf{n}(\mathbf{x}_0)\cdot\nabla G^{3D-2P}(\mathbf{x}_0, \mathbf{x})\; dS(\mathbf{x}_0) \tag{6}$$

where $\mathbf{n}$ is the unit vector pointing into the control volume, and P, B, T stand, respectively, for the surfaces of the particles, bottom, and top of the control volume (e.g. [6]). The integrals over the sides of the control volume cancel due to the inherent periodicity of the Green's function and the assumed periodicity of the concentration field, and were not included. The first and second integrals on the right-hand side of (6) are called, respectively, the single-layer and the double-layer harmonic potentine.

As the bottom of the control volume is shifted to negative infinity, the concentration tends to become constant, the Green's function decays to zero at an exponential rate, and the corresponding integrals in (6) vanish. Because the concentration over each particle surface is constant, it can be brought outside the double-layer integral, and the properties of the Green's function guarantee that the corresponding integrals vanish. As the top of the control volume is shifted to infinity, the Green's function behaves as shown in Eq. (4), and the representation (6) simplifies to

$$c(\mathbf{x}) = -\int_{P} [\mathbf{n}\cdot\nabla c](\mathbf{x}_0)\; G^{3D-2P}(\mathbf{x}_0, \mathbf{x})\; dS(\mathbf{x}_0) + \frac{q_\infty}{DA}\int_{T}(z - z_0)\; dS(\mathbf{x}_0) + \frac{1}{A}\int_{T} c(\mathbf{x}_0)\; dS(\mathbf{x}_0). \tag{7}$$

Using property (5) to switch the arguments of the Green's function within the first integral on the right-hand side of Eq. (7), we find

$$c(\mathbf{x}) = -\int_{P} [\mathbf{n}\cdot\nabla c](\mathbf{x}_0)\; G^{3D-2P}(\mathbf{x}, \mathbf{x}_0)\; dS(\mathbf{x}_0) + \frac{1}{A}\int_{P} [\mathbf{n}\cdot\nabla c](\mathbf{x}_0)\; (z - z_0)\; dS(\mathbf{x}_0) + \frac{q_\infty}{DA}\int_{T}(z - z_0)\; dS(\mathbf{x}_0) + \frac{1}{A}\int_{T} c(\mathbf{x}_0)\; dS(\mathbf{x}_0). \tag{8}$$

The sum of the last three terms may be simplified by use of the reciprocal theorem for harmonic functions written for the harmonic concentration field c and for the non-singular harmonic function $z-z_0$, yielding

$$\int_{P,\,B,\,T} [\mathbf{n}\cdot\nabla c](\mathbf{x}_0)\; (z - z_0)\; dS(\mathbf{x}_0) = \int_{P,\,B,\,T} c(\mathbf{x}_0)\cdot\mathbf{n}(\mathbf{x}_0)\; \nabla(z - z_0)\; dS(\mathbf{x}_0) \tag{9}$$

which is the counterpart of the boundary integral representation (6). Simplifying as previously, we find

$$\int_{P} [\mathbf{n}\cdot\nabla c](\mathbf{x}_0)\; (z - z_0)\; dS(\mathbf{x}_0) + \frac{q_\infty}{D}\int_{T}(z - z_0)\; dS(\mathbf{x}_0) = c_0 A - \int_{T} c(\mathbf{x}_0)\; dS(\mathbf{x}_0). \tag{10}$$

Finally, we combine Eqs. (8) and (10) to obtain the compact integral representation

$$c(\mathbf{x}) = c_0 - \int_{P} [\mathbf{n}\cdot\nabla c](\mathbf{x}_0)\; G^{3D-2P}(\mathbf{x}, \mathbf{x}_0)\; dS(\mathbf{x}_0) \tag{11}$$

which expresses the concentration field in terms of a distribution of point sources of mass deployed over the particle surfaces.

Placing the point $\mathbf{x}$ on the particle surfaces, and requiring the satisfaction of the boundary condition $c = c_0$, we obtain a homogeneous Fredholm integral equation of the first kind for the distribution of the derivative of the concentration normal to the particle surfaces. A nontrivial solution arises by requiring the global mass balance

$$-D\int_{P} [\mathbf{n}\cdot\nabla c](\mathbf{x}_0)\; dS(\mathbf{x}_0) = Aq_\infty \tag{12}$$

where A is the area of a planar cell. As a practical

alternative, we may apply the representation (11) at a point that is located far above the top layer, neglect the exponentially decaying terms, and thereby supplement the integral equation with an algebraic equation, while also introducing the additional unknown c_{D} defined in Eq. (2).

2.2. Formulation for small volume fractions

When the size of all particles is sufficiently small compared to the characteristic particle separation L, which can be identified with the smallest of the magnitudes of the base vectors $|\mathbf{a}_1|$, $|\mathbf{a}_2|$, or $|\mathbf{a}_3|$, we may approximate the Green's function within the integral over each particle on the right-hand side of (11) with a constant. This simplification provides us with the approximate representation

$$c(\mathbf{x}) = c_0 + \frac{1}{D}\sum_{l=1}^{\infty} Q_l G^{\,3\mathrm{D}-2\mathrm{P}}(\mathbf{x},\, \mathbf{x}_l) \tag{13}$$

where $\mathbf{x}_l$ is the designated center of any one particle that belongs to the lth layer, and the coefficient Q_l is the rate of mass transport from the surface of each particle that belongs to the lth layer, measured in moles per unit time.

Using property (4), we find that far above the top layer, the right-hand side of (13) produces

$$c(\mathbf{x}) \cong c_0 - \frac{1}{DA}\sum_{l=1}^{\infty} Q_l (z - z_l). \tag{14}$$

A comparison with Eq. (2) gives

$$q_\infty = \frac{1}{A}\sum_{1}^{\infty} Q_l \tag{15}$$

and

$$c_{\mathrm{D}} = c_0 - \frac{1}{DA}\sum_{1}^{\infty} Q_l \mid z_l \mid \tag{16}$$

which shows that the displacement concentration constant c_{D} is less than c_0.

To compute the rate of mass transport from each particle, we use the method of matched asymptotic expansions. First, we consider transport in the inner regime surrounding a particle, and account for the presence of all other particles by requiring an appropriate far-field boundary condition. Let h_k be the mass transfer coefficient for a solitary particle that lies in the kth layer; for a spherical particle of radius a_k, we have $h_k = D/a_k$. Then, by definition,

$$Q_k = h_k 4\pi a_k^2 (c_0 - c_k^\infty) \tag{17}$$

where c_k^∞ is the far-field value. To compute this value, we observe the limit of the right-hand side of Eq. (13) as the field point $\mathbf{x}$ approaches the designated particle center, and keep only the terms that are singular or tend to a constant value finding

$$c(\mathbf{x}) \cong \frac{Q_k}{4\pi D}\,\frac{1}{\mid \mathbf{x} - \mathbf{x}_k \mid} + \frac{Q_k}{D} d_k^\infty + \frac{1}{D}\sum_{l=1,\, l\neq k}^{\infty} Q_l\, G^{\,3\mathrm{D}-2\mathrm{P}}(\mathbf{x}_k,\, \mathbf{x}_l) + c_0 \tag{18}$$

where d_k^∞ is a lattice configuration dependent constant with dimensions of inverse length. This constant follows readily from the general expression for the Green's function to be discussed in the next section. Invoking now the general principles of matched asymptotic expansions, we identify the constant c_k^∞ with the sum of the last three terms on the right-hand side of (18). Substituting into Eq. (17) we find

$$Q_k = -\frac{h_k 4\pi a_k^2}{D}\left(Q_k d_k^\infty + \sum_{l=1,\, l\neq k}^{\infty} Q_l\, G^{\,3\mathrm{D}-2\mathrm{P}}(\mathbf{x}_k, \mathbf{x}_l)\right) \tag{19}$$

which may be rearranged to give the homogeneous equation

$$M_{kl} Q_l = 0. \tag{20}$$

We have introduced the influence matrix $\mathbf{M}$ with components

$$M_{kl} = \frac{h_k 4\pi a_k^2}{D} G^{\,3\mathrm{D}-2\mathrm{P}}(\mathbf{x}_k,\, \mathbf{x}_l) \tag{21}$$

for $k \neq l$, and

$$M_{kk} = 1 + \frac{h_k 4\pi a_k^2}{D} d_k^\infty \tag{22}$$

where summation over k is *not* implied on the left-hand side of (22).

The elements of the matrix $\mathbf{M}$ may be conveniently expressed in terms of the lattice Nusselt number defined as

$$Nu_k^{\mathrm{Lattice}} = \frac{h_k a_k^2}{DL} = Nu_k \frac{a_k}{L} \tag{23}$$

where $Nu_k = h_k a_k / D$ is the usual particle Nusselt number; for a spherical particle, $Nu_k = 1$ and $Nu_k^{\mathrm{Lattice}} = a_k/L$. Subject to the preceding definition, Eqs. (21) and (22) become

$$M_{kl} = 4\pi Nu_k^{\mathrm{Lattice}} L G^{\,3\mathrm{D}-2\mathrm{P}}(\mathbf{x}_k,\, \mathbf{x}_l) \tag{24}$$

for $k \neq l$, and

$$M_{kk} = 1 + 4\pi Nu_k^{\text{Lattice}} L d_k^{\infty}. \tag{25}$$

It is important to note that the effects of the particle shape and size have been incorporated into the lattice Nusselt number. For any particle shape, including shapes with fine indentations and fractal geometry, the lattice Nusselt number is proportional to the particle size defined with respect to the particle volume. Thus, the assumption of small particle size guarantees the smallness of the lattice Nusselt number.

Expression (17) would remain valid even if linear terms were retained on the right-hand side of expansion (13). These terms would produce an antisymmetric distribution of the concentration with respect to the three spatial coordinates, to be used as the far-field condition in solving Laplace's equation in the inner regime, and would thus make a vanishing contribution to the overall transport rate. The error associated with expressions (24) and (25) is thus on the order of $(a_k/L)^2$.

As it stands, the linear system (20) has the obvious solution $Q_l = 0$ for all values of l, but this triviality is removed by imposing an appropriate physical constraint, as discussed in the preceding subsection.

2.2.1. Decay of the transport rate down the lattice

As the ratios a_k/L tend to vanish, the upper left square block of $\mathbf{M}$ tends to become diagonal, and an asymptotic behavior is established whereupon the rate of mass transfer tends to become uniform across the top layers. We note, however, that the Green's function on the right-hand side of Eq. (24) grows linearly with the distance above a certain layer and vanishes far below the layer. Thus, in spite of the assumed smallness of the lattice Nusselt number, the right-hand side of (24) is not necessarily small for well separated layers. To establish the asymptotic behavior far below the top layer, we note that the solution of the discrete problem bears some resemblance to the solution of the integral equation

$$(1 + 4\pi L Nu^{\text{Lattice}}(w)\, \mathrm{d}^{\infty}(w))Q(w) + \frac{4\pi L}{V} Nu^{\text{Lattice}}(w) \int_{-\infty}^{w} (v - w)Q(v)\, \mathrm{d}v = 0 \tag{26}$$

where $Nu^{\text{Lattice}}(w)$ expresses the particle radii distribution down the semi-infinite matrix, $V = A \mid \mathbf{a}_3 \cdot \mathbf{e}_3 \mid$ is the volume of the unit cell, and $\mathbf{e}_3$ is the unit vector along the z axis. Approximating $Nu^{\text{Lattice}}(w)$ with a constant, neglecting it from the expression within the first set of parentheses in (26), and differentiating the resulting equation twice with respect to w, we derive an elementary second-order linear differential equation for $Q(w)$. A solution that decays as w tends to negative infinity is given by

$$Q(w) = \beta \mathrm{e}^{-\sigma|w|} \tag{27}$$

where β is an arbitrary constant, and σ is the rate of decay given by

$$\sigma = \left(\frac{4\pi L}{V} Nu^{\text{Lattice}}\right)^{1/2}. \tag{28}$$

Since the lattice Nusselt number is proportional to the equivalent particle radius which is defined as the radius of a sphere with the same volume, Eq. (28) suggests that the rate of decay σ is proportional to the particle volume fraction raised to the 1/6 power. Based on Eq. (27), we expect that the rate of transport from the particles will decrease in an exponential fashion with respect to distance from the top layer. This behavior will be confirmed by the numerical results presented in section 4.

2.2.2. Evolution of particle sizes

Having established an expression for the rate of mass transfer from the kth layer, we may derive evolution equations for the particle sizes, subject to the additional assumption that the rates of change of the particle radii $\mathrm{d}a_k/\mathrm{d}t$ are much smaller than the diffusion time a_k^2/D. When this condition is met, transport occurs through a sequence of quasi-steady states.

Assuming, for example, that the particles are, and remain, spherical with radius $a_k(t)$, which will be true in the case of evaporation of small liquid drops, or in the case of moderate sized drops with large surface tension, we write,

$$\rho_k \frac{\mathrm{d}V_k}{\mathrm{d}t} = 4\pi\rho_k a_k^2 \frac{\mathrm{d}a_k}{\mathrm{d}t} = -mQ_k(a_1, a_2, \ldots) \tag{29}$$

where V_k is the particle volume, ρ_k is the particle density, and m is the vapor phase molecular weight. Rearranging the right-hand side, we obtain the nonlinear autonomous system of ordinary differential equations

$$\frac{\mathrm{d}a_k}{\mathrm{d}t} = -\frac{m}{4\pi\rho_k a_k^2} Q_k(a_1, a_2, \ldots) \tag{30}$$

which can be solved subject an appropriate initial condition up to the time where the radius of a particle becomes equal to zero; that is, up to the time where a particle completely evaporates.

3. Computation of the Green's function

To obtain quantitative results, we require readily computable expressions for the doubly-periodic Green's function of Laplace's equation with singular points located at the nodes $\mathbf{x}_n = \mathbf{x}_0 + \mathbf{X}_n$, where $\mathbf{x}_0$ is

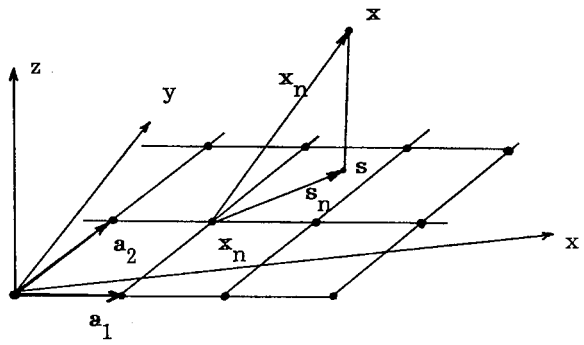

Fig. 2. Illustration of a planar lattice of singularities used to derive the doubly-periodic Green's function of Laplace's equation.

the position of any one singularity. The points $\mathbf{X}_n$ define the vertices of a two-dimensional Bravais lattice described by

$$\mathbf{X}_n = i_1\mathbf{a}_1 + i_2\mathbf{a}_2 \tag{31}$$

where i_1, i_2 are two integers, and $\mathbf{a}_1$, $\mathbf{a}_2$ are two base vectors parallel to the 12 or xy plane, as shown in Fig. 2. As the field point $\mathbf{x}$ moves far below the xy plane, the Green's function is required to vanish.

We begin by introducing the area of the dimensional unit cell $A = |\,\mathbf{a}_1 \times \mathbf{a}_2\,|$, and the reciprocal wave-number base vectors

$$\mathbf{b}_1 = \frac{2\pi}{A}\mathbf{a}_2 \times \mathbf{e}_3, \quad \mathbf{b}_2 = \frac{2\pi}{A}\mathbf{e}_3 \times \mathbf{a}_1 \tag{32}$$

where $\mathbf{e}_3$ is the unit vector along the z axis. Furthermore, we define the vertices of the reciprocal wave number Bravais lattice

$$\mathbf{l}_\lambda = j_1\mathbf{b}_1 + j_2\mathbf{b}_2 \tag{33}$$

where j_1, j_2 are two integers.

Using the method of Fourier transform, we find that the Green's function is given by

$$G^{\mathrm{3D-2P}}(\mathbf{x}, \mathbf{x}_0) = \frac{1}{A}\Bigg[-\alpha\,|\,\hat{\mathbf{x}}_0 \cdot \mathbf{e}_3\,| + \frac{1}{2}\sum_{\lambda,\,|\mathbf{l}_\lambda|\neq 0} \frac{1}{|\,\mathbf{l}_\lambda\,|}\cos(\mathbf{l}_\lambda \cdot \hat{\mathbf{x}}_0)\exp(-\,|\,\mathbf{l}_\lambda\,||\,\hat{\mathbf{x}}_0 \cdot \mathbf{e}_3\,|)\Bigg] \tag{34}$$

where $\alpha = 1$ when $\hat{\mathbf{x}}_0 \cdot \mathbf{e}_3 > 0$, and 0 otherwise, and we have introduced the distance of the field point $\mathbf{x}$ from a singular point $\mathbf{x}_n$

$$\hat{\mathbf{x}}_n \equiv \mathbf{x} - \mathbf{x}_n. \tag{35}$$

Expression (34) is useful when the field point $\mathbf{x}$ is located sufficiently *far* from the plane of the singularities, for then the exponential factors multiplying the cosines decay at a fast rate. As the observation point approaches the plane of the singular points, the accurate computation of the Fourier series requires an increasing number of terms; the method fails when the observation lies in the plane of the singularities. Clearly, the Fourier expansion is not useful for computing the field at the position of one singularity induced by all other singularities in its plane.

It is thus imperative that we develop an alternative method for computing the doubly-periodic Green's function. Several attempts have been made to compute this Green's function directly in terms of Ewald sums [2], but an indirect method developed by Hautman and Klein [7] in the context of molecular fields is the best performer. We begin by defining the projection $\mathbf{s}$ of the field point $\mathbf{x}$ onto the plane of the singularities, as shown in Fig. 2, and introduce the distance of the projection from a singular point $\mathbf{x}_n$,

$$\hat{\mathbf{s}}_n \equiv \mathbf{s} - \mathbf{x}_n. \tag{36}$$

The Green's function is computed in five parts, as follows:

$$G^{\mathrm{3D-2P}}(\mathbf{x}, \mathbf{x}_0) = -\frac{\alpha}{A}\,|\,\hat{\mathbf{x}}_0 \cdot \mathbf{e}_3\,| + \frac{1}{4\pi}\left(R(\mathbf{x}, \mathbf{x}_0) + S_0 - \frac{1}{2}\,|\,\hat{\mathbf{x}}_0 \cdot \mathbf{e}_3\,|^2\, S_1 + \frac{3}{8}\,|\,\hat{\mathbf{x}}_0 \cdot \mathbf{e}_3\,|^4\, S_2 \right) \tag{37}$$

where

$$R(\mathbf{x}, \mathbf{x}_0) = \sum_n \left(\frac{1}{|\,\hat{\mathbf{x}}_n\,|} - \frac{1}{|\,\hat{\mathbf{s}}_n\,|} + \frac{1}{2}\,\frac{|\,\hat{\mathbf{x}}_0 \cdot \mathbf{e}_3\,|^2}{|\,\hat{\mathbf{s}}_n\,|^3} - \frac{3}{8}\,\frac{|\,\hat{\mathbf{x}}_0 \cdot \mathbf{e}_3\,|^4}{|\,\hat{\mathbf{s}}_n\,|^5} \right) \tag{38}$$

and the summation is over all singularities. The summed terms on the right-hand side of (38) decay like $1/|\hat{\mathbf{s}}_n|^7$, and this allows for an expedient numerical summation. When, in particular, the observation point $\mathbf{x}$ lies in the plane of the singularities, $R(\mathbf{x}, \mathbf{x}_0)$ is identically equal to zero and does not need to be computed. More generally, the indices i_1 and i_2 introduced in Eq. (31) for summation in the plane of the singularities on the right-hand side of (38), may be truncated at an appropriate level that depends on the distance of the observation point from the plane of the singularities.

The rest of the functions that appear on the right-hand side of Eq. (37) are defined as follows:

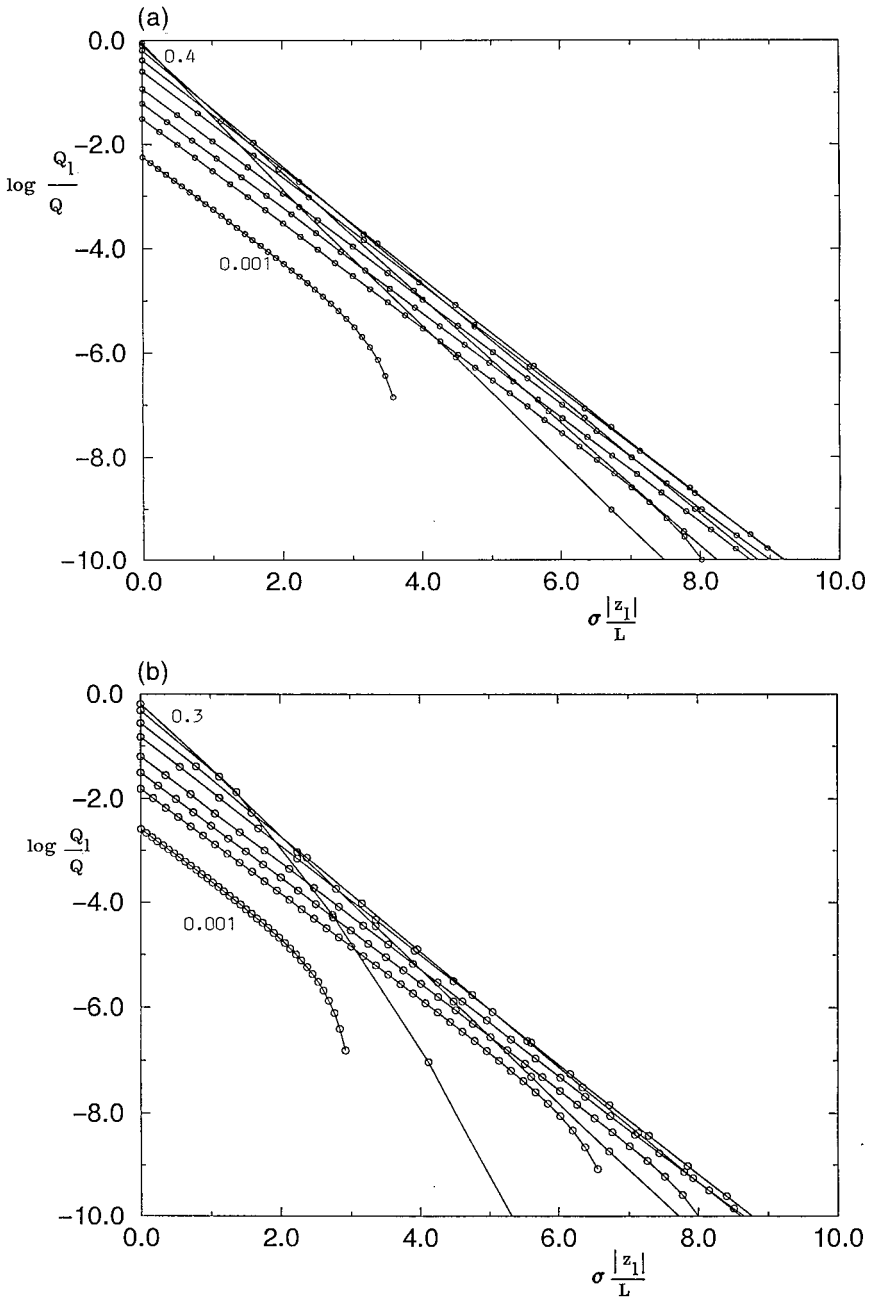

Fig. 3. Transport through a semi-infinite lattice of identical particles with radius a, for various lattice Nusselt numbers. Graphs of the fractional rate of transport beneath the top layer for: (a) a simple cubic lattice described by $\mathbf{a}_1 = L\mathbf{e}_1$, $\mathbf{a}_2 = L\mathbf{e}_2$, $\mathbf{a}_3 = L\mathbf{e}_3$, for $Nu^{\text{Lattice}} = 0.001$, 0.005, 0.01, 0.02, 0.05, 0.1, 0.2, 0.3, 0.4; (b) a body-centered cubic lattice described by $\mathbf{a}_1 = L\mathbf{e}_1$, $\mathbf{a}_2 = L\mathbf{e}_2$, $\mathbf{a}_3 = 0.5L\,(\mathbf{e}_1 + \mathbf{e}_2 + \mathbf{e}_3)$, for $Nu^{\text{Lattice}} = 0.001$, 0.005, 0.01, 0.02, 0.05, 0.1, 0.2, 0.3.

$$S_0 = \sum_n \frac{1 - H_0(\xi \mid \hat{\mathbf{s}}_n \mid)}{\mid \hat{\mathbf{s}}_n \mid} + \frac{2\pi}{A}\left[-\frac{1}{\sqrt{\pi}\xi} + \sum_{\substack{\lambda \\ \mid \mathbf{l}_\lambda \mid \neq 0}} \cos(\mathbf{l}_\lambda \cdot \hat{\mathbf{x}}_0) \frac{1}{\mid \mathbf{l}_\lambda \mid} \operatorname{erfc}\left(\frac{\mid \mathbf{l}_\lambda \mid}{2\xi} \right) \right] \tag{39}$$

$$S_1 = \sum_n \frac{1 - H_1(\xi \mid \hat{\mathbf{s}}_n \mid)}{\mid \hat{\mathbf{s}}_n \mid^3} - \frac{2\pi}{A} \sum_{\substack{\lambda \\ \mid \mathbf{l}_\lambda \mid \neq 0}} \cos(\mathbf{l}_\lambda \cdot \hat{\mathbf{x}}_0) \mid \mathbf{l}_\lambda \mid \operatorname{erfc}\left(\frac{\mid \mathbf{l}_\lambda \mid}{2\xi} \right) \tag{40}$$

$$S_2 = \sum_n \frac{1 - H_2(\xi \mid \hat{\mathbf{s}}_n \mid)}{\mid \hat{\mathbf{s}}_n \mid^5} + \frac{2\pi}{A} \frac{1}{9} \sum_{\substack{\lambda \\ \mid \mathbf{l}_\lambda \mid \neq 0}} \cos(\mathbf{l}_\lambda \cdot \hat{\mathbf{x}}_0) \mid \mathbf{l}_\lambda \mid^3 \operatorname{erfc}\left(\frac{\mid \mathbf{l}_\lambda \mid}{2\xi} \right) \tag{41}$$

where ξ is an Ewald summation parameter determining the balance between the sums in real space and wave number space on the right-hand sides of the preceding three equations. The splitting functions H_0, H_1, H_2 within the real-space sums on the right-hand side of Eqs. (39)–(41) are given by

$$H_0(w) = \operatorname{erf}(w) \tag{42}$$

$$H_1(w) = \operatorname{erf}(w) - \frac{2}{\sqrt{\pi}} w(1 + 2w^2) \exp(-w^2) \tag{43}$$

$$H_2(w) = \operatorname{erf}(w) - \frac{2}{\sqrt{\pi}} w\left(1 + \frac{2}{3}w^2 - \frac{4}{9}w^4 + \frac{8}{9}w^6\right) \exp(-w^2) \tag{44}$$

where erf is the error function. The Gaussian decay of these functions, combined with the Gaussian decay of the complementary error function on the right-hand side of (39)–(41), are crucial for the success of the numerical method. The results are, and have been confirmed to be, independent of ξ, with the optimal value for the least computational effort depending on the lattice geometry. In practice, with the optimal choice, the indices i_1 and i_2, defined in Eq. (31) for summing in real space, and the indices j_1 and j_2, defined in Eq. (33) for summing in wave number space, are truncated at a moderate level on the order of five.

The second method of computing the Green's function is useful when a field point is located near, or lies in the plane of the singularities. As the field point moves away from the plane of the singularities, the Fourier series method described earlier becomes more efficient.

4. Results and discussion

In the numerical computations, we specify the overall rate of mass transfer from each planar cell $Q = Aq_\infty$, and truncate the linear system (20) at a certain level NLR. We then arbitrarily specify the value of Q_{NLR}, and solve the top NLR−1 equations for Q_l, $l = 1, \ldots,$ NLR−1, by the method of Gauss elimination. Having produced the solution, we normalize it to satisfy the constraint (15). Numerical difficulties were not encountered, apart for numerical underflow occurring when a large number of layers with rapidly decaying rates of transport were retained.

First, we discuss results on the rate of transport from a lattice of identical particles, for a range of the lattice Nusselt number Nu^{Lattice} defined in Eq. (23). We recall that for a spherical particle of radius a, $Nu^{\mathrm{Lattice}} = a/L$. In Fig. 3, we plot the logarithm of the fractional rate of transport Q_l/Q against the reduced distance from the top layer $\sigma|z_l|/L$, where the theoretical rate of decay σ was defined in Eq. (28). Fig. 3(a) corresponds to a simple cubic lattice described by $\mathbf{a}_1 = L\mathbf{e}_1$, $\mathbf{a}_2 = L\mathbf{e}_2$, $\mathbf{a}_3 = L\mathbf{e}_3$, and the curves correspond to $Nu^{\mathrm{Lattice}} = 0.001$, 0.005, 0.01, 0.02, 0.05, 0.1, 0.2, 0.3, 0.4, shifted upwards in this progression. Fig. 3(b) corresponds to a body-centered cubic lattice described by $\mathbf{a}_1 = L\mathbf{e}_1$, $\mathbf{a}_2 = L\mathbf{e}_2$, $\mathbf{a}_3 = 0.5L(\mathbf{e}_1 + \mathbf{e}_2 + \mathbf{e}_3)$, and the curves correspond to $Nu^{\mathrm{Lattice}} = 0.001$, 0.005, 0.01, 0.02, 0.05, 0.1, 0.2, 0.3, shifted upwards in this progression. Note that for the highest value of Nu^{Lattice}, the particulate nature of the matrix is apparent.

Eq. (27) predicts that for small Nu^{Lattice}, as $|z_l|$ tends to infinity, the graphs in Fig. 3 will tend to become straight lines with slope equal to −1. Not only is this reproduced by the numerical solution, apart from the curved tail-ends due to numerical truncation, but also the exponential decay describes almost the whole of the distribution up to the top layer. For both lattice types described in Fig. 3, as Nu^{Lattice} becomes smaller, the magnitude of Q_l/Q near the interface is reduced because more layers contribute to the rate of transport. For example, for the simple cubic lattice represented by Fig. 3(a), when $Nu^{\mathrm{Lattice}} = 0.01$, it takes approximately ten layers for the rate of transport to decrease by one order of magnitude. As Nu^{Lattice} is raised, the top layers shield the lower ones, and Q_l/Q shows a first decay.

Comparing corresponding curves in Fig. 3(a) and (b), we observe similar behaviors, with quantitative differences present but not prominent. For a certain value of Nu^{Lattice}, the rate of transport from the top layer of the simple cubic lattice is higher than that of

the body-centered cubic lattice; correspondingly, a lower number of layers contribute to the overall rate of transport. Similar behavior was observed for different lattice types including the orthorhombic and the hexagonal.

Having established the physical relevance of the exponential form (27), we may introduce an average concentration $\langle c\rangle$ and compute it by solving the following one-dimensional diffusion equation with an appropriate source term included

$$D\frac{\mathrm{d}^2\langle c\rangle}{\mathrm{d}z^2} + Q\sigma\ \exp(\sigma z) = 0 \tag{45}$$

where $-\infty < z < 0$. The solution is

$$\langle c\rangle = c_0 - \frac{Q}{D\sigma}\exp(\sigma z) \tag{46}$$

which illustrates the exponential decay of the average field down the semi-infinite matrix. Above the matrix, the average field increases linearly with distance yielding a composite profile. Combining the preceding two equations we find

$$\frac{\mathrm{d}^2\langle c\rangle}{\mathrm{d}z^2} - \sigma^2(\langle c\rangle - c_0) = 0 \tag{47}$$

which is similar to Brinkman's equation describing the flow near the surface of a porous medium [2].

Next, we consider the evolution of spherical particles due to evaporation, governed by Eq. (30). In the numerical computations, a finite number of particle layers on the order of twenty were retained, and the ordinary differential equations were integrated in time using the second-order Runge–Kutta method with a constant time step. The equation for the top layer was removed from the truncated system when the corresponding particle radii have vanished. At the initial instant, all particles were assumed to have a uniform radius a_0.

In Fig. 4(a), we plot the particle radii a/L against reduced time $\hat{t} = mQt/(\rho L^3)$ for the simple cubic lattice described in a previous paragraph, and for $a_0/L = 0.1$. Successive curves correspond to adjacent particle layers. The numerical results show that a periodic state is rapidly established in which the top particles evaporate, only to be replaced by particles residing in the next layer. The period T between the time where a particle has reached the top and the time where it has completely disappeared, is equal to the distance between two successive zero crossings in Fig. 4(a), following the initial transition period. We note that, after the periodic state has been established, one particle per surface cell completely evaporates within the time T, and this suggests

$$T = \frac{\rho}{mQ}\frac{4\pi}{3}a_0^3 \tag{48}$$

or in dimensionless form, $\hat{T} = mQT/(\rho L^3) = (4\pi/3)(a_0/L)^3$. This value is recovered with high precision from the results of the numerical computations.

After the periodic state has been established, the distribution of the particle radii down the semi-infinite matrix becomes a periodic function of time. This distribution arises by locating the intersections between the curves in Fig. 4(a) and a vertical line drawn at a certain time. In Fig. 4(c), we plot, with filed circles, the radii of successive layers at the time when the top layer has just disappeared, and observe a rapid decay. At that time, the radii of the top particles are roughly 77% of those of the particles in the fifth layer, and the latter is very close to the radii of the particles deep down the matrix.

Similar results were obtained for different volume fractions and lattices with different geometry. As an example, in Fig. 4(b) we plot the particle radii a/L against reduced time $\hat{t} = mQt/(\rho L^3)$ for the body-centered cubic lattice described previously. In Fig. 4(c), we plot with solid squares, the radii of successive layers at the time where the top layer has just vanished. Because a larger number of layers contribute to the rate of transport at any instant, as seen in the graphs presented in Fig. 3, the square symbols in Fig. 4(c) lie underneath the circles, yielding a more gradual transition to the deep-matrix radii.

5. Conclusions and discussion

We have developed an integral formulation that describes the rate of transport from a semi-infinite lattice of particles, and performed an asymptotic expansion to study the behavior in the limit of small volume fractions. An important aspect of the integral formulation is the use of the doubly-periodic Green's function of Laplace's equation which was computed in the form of a rapidly converging series developed by Hautman and Klein [7]. This Green's function arises in a variety of contexts including electrostatics, convective transport, potential flow, and creeping flow. Results of numerical computations confirmed the exponential decay of the rate of transport with distance from the interface, and illustrated the distribution of the particle size near the interface of an evaporating matrix. The lattice geometry was seen to play a secondary role in determining the qualitative features of transport.

To study conductive transport from particles with moderate and large size, as well as transport from particles with evolving shapes, it is necessary to solve the integral equation for the distribution of the flux over the particle surfaces developed in section 2 using a nu-

merical method. Two possibilities are the boundary element method [6] and the method of multi-pole expansions [2]. Previous experience with similar problems suggests that for fixed particle geometry, the asymptotic results derived in this paper provide us with accurate predictions for particles whose radius is comparable to, or less than half the particle separation [8]. It would be reassuring, however, to confirm this expectation by use of numerical methods.

The formulation in section 3 may be extended in a straightforward manner to describe shear flow over the surface of the semi-infinite particle lattice illustrated in Fig. 1, modeling an ordered semi-infinite porous medium. At vanishing Reynolds number, the motion of the fluid is governed by the linear equations of Stokes flow including the continuity equation and the Stokes equation:

$$\nabla \cdot \mathbf{u} = 0, \qquad -\nabla p + \mu \nabla^2 \mathbf{u} = 0 \tag{49}$$

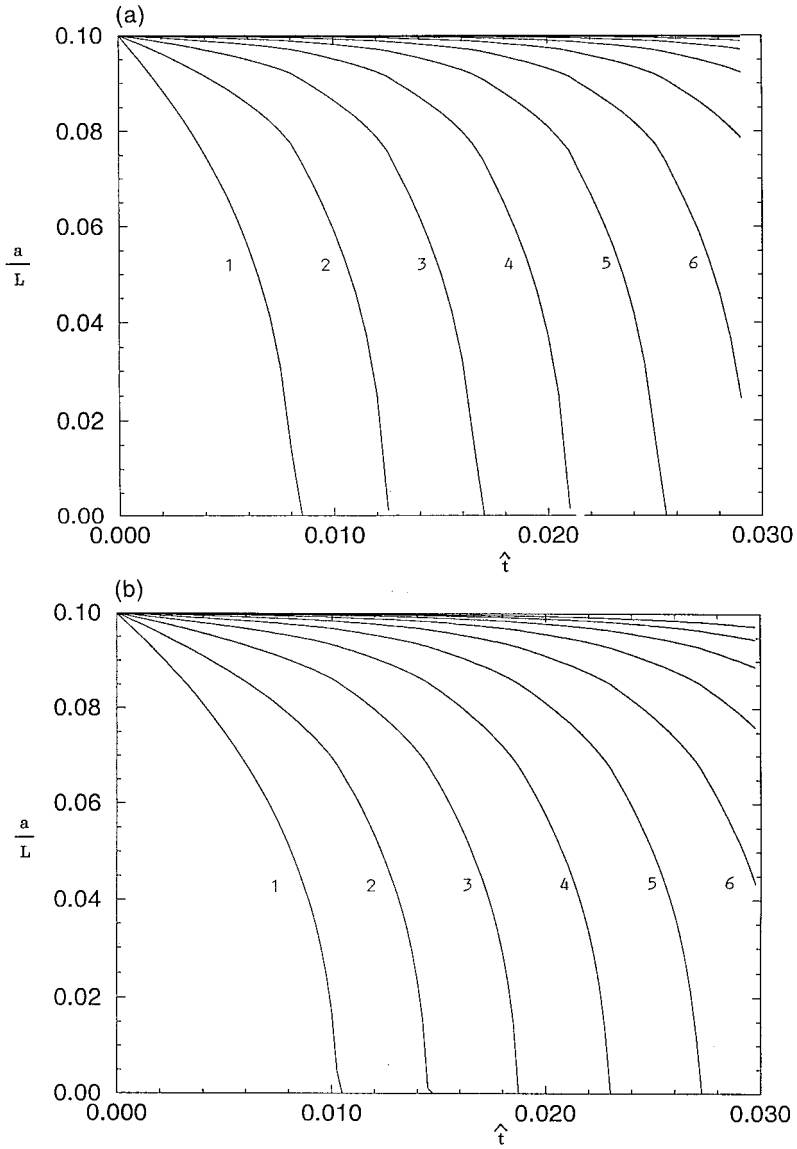

Fig. 4. Evolution of the particle radii a/L with respect to reduced time $\hat{t} = mQt/(\rho L^3)$ for successive layers corresponding to (a) the simple cubic lattice, and (b) the body-centered cubic lattice. (c) Distribution of particle radii at the time when the top layer has disappeared; the filled circles are for the simple cubic lattice, and the filled squares are for the body-centered cubic lattice.

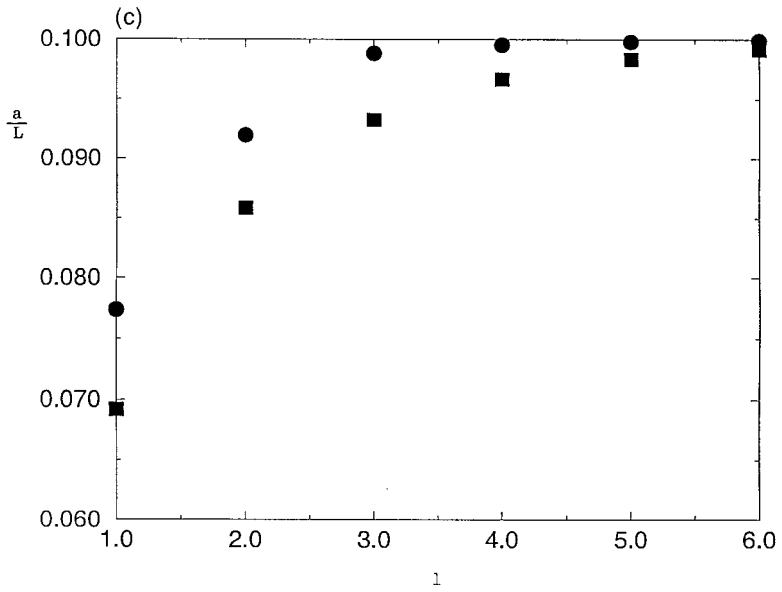

Fig. 4 (*continued*)

where $\mathbf{u}$ is the fluid velocity, p is the pressure, and μ is the fluid viscosity [e.g. 6]. Far above the top layer, the velocity obtains the asymptotic form $\mathbf{u}^{\infty} = (kz\mathbf{e} + \mathbf{u}^{\text{slip}})$, where k is the constant shear rate, $\mathbf{e}$ is a unit vector parallel to the xy plane, and $\mathbf{u}^{\text{slip}}$ is a slip-velocity corresponding to the designated origin of the z axis. An integral formulation for the problem of shear flow is presented in [8] along with an asymptotic analysis for small particle sizes and numerical solutions for flow over a single particle layer representing a porous plate.

Acknowledgements

This research was supported by the National Science Foundation. Acknowledgment is made to the Donors of the Petroleum Research Fund, administered by the American Chemical Society, for partial support.

References

[1] G.I. Batchelor, Transport properties of two-phase materials with random structure, Ann. Rev. Fluid Mech. 6 (1974) 227–255.
[2] A.S. Sangani, S. Behl, The planar singular solutions of Stokes and Laplace equations and their application to transport processes near porous surfaces, Phys. Fluids A 1 (1989) 21–37.
[3] W.L. Keey, Drying: Principles and Applications, Pergamon Press, London, 1972.
[4] R.E. Larson, J.J.L. Higdon, Microscopic flow near the surface of two-dimensional porous media. 1. Axial flow, J. Fluid Mech. 166 (1986) 449–472.
[5] R.E. Larson, J.J.L. Higdon, Microscopic flow near the surface of two-dimensional porous media. 2. Transverse flow, J. Fluid Mech. 178 (1987) 119–136.
[6] C. Pozrikidis, Introduction to Theoretical and Computational Fluid Dynamics, Oxford University Press, New York, 1977.
[7] J. Hautman, M.L. Klein, An Ewald summation method for planar surfaces and interfaces, Molecular Physics 75 (1992) 379–395.
[8] C. Pozrikidis, Shear flow over a particulate or fibrous plate, Submitted for publication (1999).